First Principles Study on 2H-1T' Transition in MoS2 with Copper

Journal:	*Physical Chemistry Chemical Physics*
Manuscript ID	CP-ART-08-2018-005445.R2
Article Type:	Paper
Date Submitted by the Author:	30-Sep-2018
Complete List of Authors:	Huang, H. H.; Jilin University, School of Materials Science & Engineering Fan, Xiaofeng; Jilin University, College of Materials Science and Engineering Singh, David; University of Missouri, Department of Physics and Astronomy Zheng, Wei Tao; Jilin University, School of Materials Science & Engineering

First Principles Study on 2H-1T' Transition in MoS_2 with Copper

H.H. Huang[a], Xiaofeng Fan[a,*], David J. Singh[c] and W.T. Zheng[a,b,†]

a. *Key Laboratory of Automobile Materials (Jilin University), Ministry of Education, and College of Materials Science and Engineering, Jilin University, Changchun 130012, China*

b. *State Key Laboratory of Automotive Simulation and Control, Jilin University, Changchun 130012, China*

c. *Department of Physics and Astronomy, University of Missouri, Columbia, Missouri 65211-7010, USA*

*,†Correspondence and requests for materials should be addressed, xffan@jlu.edu.cn (X. Fan); wtzheng@jlu.edu.cn (W.T. Zheng)

Abstract

The electronic properties of MoS_2 are strongly controlled by structure providing a route to their modulation. We report, based on first principles calculations, that the adsorption of metal atom Cu on surface can induce the phase transition of MoS_2 from the semiconducting 2H to the metallic 1T' phase. Cu-adsorption results in effective n-type doping of the MoS_2 by charge transfer from the Cu in the case of the 1T' phase. This is distinct from the behavior on the 2H phase, where Cu does not donate charge, and also distinct from alkali metal adsorption, where charge is donated to both 2H and 1T' MoS_2. The charge donation to the 1T' phase by Cu stabilizes it with respect to the 2H structure, and importantly also reduces the energy barrier between the 2H and 1T' structures. This difference reflects the higher electronegativity of Cu, which also means that Cu modified MoS_2 can be expected to be less chemically reactive than MoS_2 with alkali metal adatoms. The main atomic mechanism of structural transition is the gliding of S atoms on upper surface. Finally, we report the energetics of the 2H to 1T' transition with several other adatoms, Ag, Au, Ni, Pt and Pd, but none of these is as effective as Cu in inducing the transition.

Keywords: phase transformation, first principles calculations, monolayer MoS_2, energy barrier

1. Introduction

Transition metal dichalcogenides (TMDs) have received considerable attention in part due to their promising potential for applications, for example, field effect transistors with high on/off ratios[1-5], spintronics[6], photovoltaics[7,8] and heterogeneous catalysis[9-12]. These layered bulk TMDs materials can also be produced as single or few layer 2D materials through mechanical exfoliation, chemical exfoliation, CVD growth and other methods[7,13,14]. These materials show strong tunability of electrical, optical and other properties in combination with good mechanical and chemical stability, as in prototypical MoS_2. This compound forms in different phases characterized by different coordination structures (trigonal prismatic and octahedral) and stacking orders, forming for example the 1T', 2H and 3R-phases[15-17]. These have very different electronic properties. Considerable attention has been focused on the modulation of electronic properties by different ways, such as alloying, doping, pressure, and so on[18-21]. An important strategy is to modify electronic properties is to induce transitions between the phases to modulate properties. Approaches include strain engineering[22], charge doping[23-25], electrostatic gating[26] and alkali metal adsorption[27]. Besides changes in electronic structure, such transitions can also modulate catalytic activity[25].

The most commonly studied structure of MoS_2 and related phases ($MoSe_2$, $MoTe_2$, WSe_2, etc.) is the ground state hexagonal phase (2H), which has trigonal prismatic coordination and semiconducting characteristics, while octahedral coordinated phases (1T) are metals or semimetals. This octahedral phase (1T) is unstable and spontaneously converts into a distorted octahedral phase (1T')[28,29]. Inducing, understanding and manipulating transitions between the 2H and 1T' structures is a very active area of research. This includes investigation of the

transformation process in single-layer MoS_2 using scanning transmission electron microscopy[30] and theoretical simulations indicating that the phase change results from the simultaneous movement of metal and chalcogenide atoms in their planes[31]. The transition has also been found in MoS_2 based Li ion batteries due to extra charge transfer accompanying Li intercalation. Phase transitions induced by electronic excitation in $MoTe_2$ were proposed[32]. There have also been studies showing phase changes stabilized by adsorption onto monolayer TMDs[33,34]. For example, it is found that adsorption of alkali metal atoms make 1T' phase more stable while molecular adsorption sustains the 2H phase[33].

Here we study the adsorption of Cu, which is very much less electropositive than the previously studied alkali metals, and additionally is much less chemically reactive. This is important for handling and characterization of materials, as well as any future device applications. We find nonetheless that the 2H – 1T' transformation on monolayer MoS_2 can be induced by the adsorption of copper and controlled via the amount of Cu adsorbed. We also find that the mechanism is distinct from that in the case of alkali metal adsorption. The microscopic dynamic processes and potential barrier are analyzed, showing that not only the 1T' structure is stabilized but the energy barrier is reduced. The origin of this effective destabilization of 2H phase is elucidated in terms of the electronic structure. We find that in contrast to alkali metals, Cu does not donate charge to 2H MoS_2. It does, however, donate charge to 1T' MoS_2 providing a relative stabilization of the 1T' phase. We also performed calculations for several possible adatoms near Cu in the periodic table, specifically, Ag, Au, Ni, Pt and Pd, and find that none of these is as effective as Cu in inducing the 2H – 1T' transition of MoS_2.

2. Computational methods

Our calculations were carried out using projector-augmented wave (PAW) pseudopotentials, as implemented in the Vienna Ab-initio Simulation Package (VASP)[35]. We used the generalized gradient approximation (GGA) of the Perdew-Burke-Ernzerhof (PBE)[36]. The kinetic energy cutoff was set to 500 eV. The zone sampling was done with a k-point grid of spacing of 0.02 $Å^{-1}$ generated by the Monkhorst-Pack scheme[37]. The energy convergence criterion was set to be 10^{-6} eV and the atomic relaxations were carried out until the forces were smaller than 0.01 $eVÅ^{-1}$. Spin polarization was considered for all the cases. In order to consider dispersion force, we added the calculations about the adsorption of different metals on MoS_2 with optPBE-vdW functional where the exchange functional was optimized for the correlation part with the consideration van der Waals (vdW) effect[38,39]. In order to accurately estimate the band gaps, we also considered the hybrid functional With HSE06[40].

Our calculated lattice constant of 3.18Å for a pristine 2H-MoS_2 monolayer is consistent with experiment and other theoretical calculations[41]. Both 2H phase (space group *P-6m2*) and 1T phase (space group *P-3m1*) have hexagonal symmetry. As shown in prior work,[29] the 1T structure is unstable and converts into the lower symmetry 1T' phase (space group $P2_1/M$)[42]. The primitive cell is doubled and becomes rectangular. Our calculated 1T' lattice constants are a = 3.177Å and b = 5.722 Å. We constructed a series of rectangular supercells (1x1, 2x1, 3x1, 4x1 and 4x2) based on the1T' primitive cell in order to simulate the Cu adsorption at different concentrations. For consistency, we also used doubled rectangular cells for our models of the 2H phase. The vacuum layers were larger than 18Å, which is sufficient to eliminate spurious interactions between layers. As an example illustrating the cells, the most favorable one adatom

configurations in the 2x1 rectangular supercells with 2H and 1T' structures are depicted in Fig.1a and 1b.

3 Results and discussion

3.1 Phase transition and dynamical barrier

We start with identification of the most stable adsorption position for Cu on MoS_2. We consider three possible high-symmetry sites including the top of Mo atom, top of S atom and center of hexagon (hollow site) for 2H phase. Based on the 1x1 rectangular cell with Cu adsorption, the results show that the adsorption energy on the top of Mo atom is approximately 0.13 eV lower than on the hollow site and 0.25 eV lower than the top of S atom. For the 1T' phase, two possible sites including the top of Mo atom and the top of S atom are examined. The adsorption energy on the top of Mo atom is about 0.37 eV lower than that on the top of S atom. Therefore, we conclude that the top of Mo atom (T_{Mo}) is the most energetically favorable position for the adsorption of Cu atom on MoS_2, regardless of whether it is in the 2H or 1T' structure.

To estimate the stability of the Cu-MoS_2 system by following the change of Cu concentration, we define the two parameters including the formation energy and adsorption energy. The formation energy per formula unit is

$$E_f = 1/n[E_{Cu_m(MoS_2)_n} - nE_{MoS_2} - mE_{Cu-bulk}], \quad (1)$$

and the adsorption energy with an atomic Cu reference is

$$E_a = 1/m[E_{Cu_m(MoS_2)_n} - nE_{MoS_2} - mE_{Cu-atom}], \quad (2)$$

where $E_{Cu_m(MoS_2)_n}$ E_{MoS_2} ,and $E_{Cu-bulk}$, are the energies of adsorption system Cu-MoS_2, pristine MoS_2 monolayer, and the energy per atom of bulk face-centered cubic Cu, respectively. $E_{Cu\text{-}atom}$ is the energy of an isolated Cu atom.

The formation energy of Cu adsorption on the 2H-MoS_2 and 1T'-MoS_2 as a function of Cu concentration is plotted in Fig. 2a. The result shows that the formation energy is positive for both phases and that the formation energy increases with increasing Cu concentration. This is a typical phenomenon in a lot of 3D semiconductor alloys. It implies that the phase separation between Cu and MoS_2 and Cu is difficult to enter into the lattice of MoS2 to replace the Mo atom. From the adsorption energy in Fig. 2b, the large negative value per adsorption atom indicates that Cu can be readily adsorbed on MoS_2, while the positive formation energy with respect to bulk Cu, suggests that this process is controllable. The first main result is that the adsorption strength of Cu on 1T' phase is significantly larger than on 2H phase. This implies that the adsorption of Cu can shift the energetic balance away from the 2H phase. As shown in Fig. 3b, at adsorption concentrations above than 13%, the 1T' phase becomes to be more stable than 2H phase.

This change is not due to strain effects. It has been reported that the TMDs, such as $MoTe_2$ and WTe_2, may undergo 2H – 1T' transitions under the applied strain. The strain effect is considered in the present case in Fig. 3b. It is found that the adsorption concentration of Cu for phase transition of MoS_2 is does not significantly change under applied strain. Therefore, mechanical deformation has a little effect on the phase transformation of MoS_2 induced the adsorption of Cu. Instead it has an electronic origin as discussed below, following discussion of the structural aspects of the transformation.

The 2H-1T' structural transformation can be understood as due to the relative gliding of different atomic planes. In the 2H-1T' transformation, the S atoms in upper plane of both S planes glide and pass though the bridge between the nearby Mo atoms to reach the position in 1T' phase, accompanied by the localized motion of Mo, as shown in Fig. 3a. In addition, all the S atoms in both S planes also have local motions along z (see Fig. 3), following the gliding of S atoms in upper plane along *x*-*y* (see Fig. 3). We analyzed the energy barrier and path way by controlling the gliding of S atoms in rectangular 1x1cells with 2 formula units of MoS_2 as depicted in Fig. 3a.The energy barrier from 2H to 1T' is approximately 1.3 eV per formula unit without Cu. With the estimated critical value of Cu for energetically destabilizing the 2H structure relative to 1T', the barrier drops to 0.9 eV per formula unit (Fig 3c). However, the barrier does not show further significant changes with further adsorption concentration increases.

3.2 Electronic properties of MoS_2 monolayer with copper adsorbed

The origin of the destabilization of the 2H structure with Cu adsorption can be understood in terms of the electronic structure. The total density of states for 2H-MoS_2 and 1T'-MoS_2 monolayers with different concentrations of adsorbed copper are shown in Fig.4a and Fig.5a, respectively. There is a clear energy gap for the 2H phase as expected. This gap gradually decreases when the adsorption concentration increases from 4% to 10%. The Fermi level goes into the conduction band as the adsorption concentration increases. In the meantime the states near the conduction band edge take on Cu character, with Mo_d hybridization. In the case of pristine 2H-MoS_2, both the conduction band minimum (CBM) and the valence band maximum (VBM) are primarily from d orbitals of Mo atoms and with a direct band gaps of 1.68 eV (Fig. S1 of SI) at PBE level. While introducing copper atoms on the surface of 2H-MoS_2, the states

near the Fermi level is mainly contributed from the s orbital of Cu adatoms as the adsorption concentration is 2% (Fig.S2a and Fig. S3a in SI). The electron count fixes the Fermi energy leading to partial occupation of the Cu s orbital as in Cu metal. With the increase of adsorption concentration, the s orbitals of Cu are broadened and hybridized with the states from conduction bands (Fig. 4b and 4c). Due to the strong coupling of s orbitals of Cu and conduction bands, the HSE doesn't change obviously the result of PBE about the conduction bands for Cu adsorption. While the band gap between valance bands and conduction bands is underestimated obviously. At PBE level, the band gaps of 2H-MoS_2, and Cu-adsorbed 2H-MoS_2 with the concentration of 7.7% and 14.3% are 1.67 eV, 1.26 eV and 0.84 eV, respectively. With HSE functional, the band gaps are 2.14 eV, 1.66 eV and 1.22 eV, respectively (Fig. S8 and S9 of SI). When the concentration of Cu adatoms exceeds 14.3%, the distribution of electronic structure is noticeably changed and the localized states appear between -0.5eV and -1eV when the adsorption concentration is 20%, which is mainly contribution from the Mo_d and Cu_d orbital (Fig.S2 and Fig. S3 in SI). At this high adsorption concentration, the bond length (2.47 Å) between Mo and S around Cu adatoms is larger than that of pristine MoS_2 (2.41 Å), meanwhile the lattice is slightly distorted.

For the case of 1T'-MoS_2 with the adsorbed Cu as illustrated in Fig.5, the total density of states indicate the Fermi level is shifted up, compared with pristine 1T'-MoS_2. This can be attributed to the electron transfer from the adatom Cu to the host. Combined with Bader charge analysis[38] as listed in Table 1, there is more charge transfer between the adsorbed Cu atom and the 1T' phase, since there are a lot of unoccupied states under the Cu_s orbital for 1T'-MoS_2. Thus the 2H and

1T' phases behave very differently in terms of charge transfer from Cu to MoS_2, with much larger transfer in the 1T' case. This can be understood in terms of the electronic structure.

The basic features of the MoS_2 electronic structure can be understood in terms of a nominal ionic model, based on Mo^{4+} and S^{2-}. From a purely electrostatic point of view octahedral coordination is favored due to packing. However, the crystal field favors a distorted trigonal prismatic coordination, as in the observed 2H phase. In the trigonal prismatic coordination the lowest Mo_d crystal field level is from the practically non-bonding z^2 orbital, while the higher levels are from antibonding combinations of S_p and Mo_d orbitals. These make up the conduction bands. This antibonding nature is strong as evidenced by the sizable band gap between the non-bonding z^2 valence band and the antibonding conduction bands. Transfer of charge from Cu would require occupation of disfavored antibonding conduction bands, and this is the explanation for the weak charge transfer and occupation of new Cu_s bands at the bottom of the conduction band. This is in contrast to alkali metal adsorption, in which case the highly electropositive atoms do donate charge to the MoS_2 sheets leading to occupation of the antibonding conduction band states. In an octahedral coordination the primary Cu_d crystal field is between a lower lying t_{2g} manifold derived from weakly antibonding states (S_p – Mo_d π^*) and an upper lying e_g set of antibonding states from S_p-Mo_d σ bonds. The lower manifold can contain six electrons, while Mo^{4+} has two. This favors the 2H structure over the octahedral coordinated phases, and also favors distortion in the 1T structure due to the partial occupation of the t_{2g} manifold. The key point is that adding electrons in the octahedral coordinated structure (1T and 1T') does not require occupation of antibonding states. This transfer is the origin for the stronger bonding of

Cu to the 1T' structure and thus the relative destabilization of the 2H structure. This is also seen in the band structures.

The projected band structure of Cu-adsorbed 2H(1T')-MoS_2 with atomic concentrations of 7.7% and 14.3% are shown in Fig. 6. The energies of Cu_d states are lower than those of Mo_d. Therefore, in Cu-adsorbed 2H-MoS_2, the valance band edges remain mainly from the Mo_d orbitals. Due to the separation between Cu_d and Mo_d, the valance band edges are not strongly disturbed relative to pristine 2H-MoS_2 (Fig. S1a). Cu-adsorbed 1T'-MoS_2 behaves similarly. The states near Fermi level are mainly from Mo_d states.

In order to analyze the charge distribution between Mo atom and S atom for the adsorption system, we calculate the charge density difference with the formula,

$$\Delta\rho(r) = \rho_{\text{total}}(r) - \rho_{Mo}(r) - \rho_{S}(r) - \rho_{Cu}(r), \quad (3)$$

where ρ_{total}, ρ_{Mo}, ρ_S and ρ_{Cu} represent the distributions of charge densities of Cu-adsorbed MoS_2, Mo atoms, S atoms and Cu atoms in real space, respectively. The charge density difference for the Cu-adsorbed MoS_2 with pristine MoS_2 is illustrated in Fig.7. For the pristine 2H and 1T'-MoS_2, there is an obvious electronic accumulation between Mo and S atom. Due to the different coordination of the 1T' phase, the z^2 orbital is not occupied and the electron charges on S along z axis disappear, compared with that of 2H phase (Fig. 7a and 7d). With the adsorption of Cu, the region of charge depletion (signed by blue color) in Mo-S lattice matrix is decreased due to the charge transfer from Cu to MoS_2. Compared with the bonding of Mo-S, the bonding of Cu-S bonding is weak, as may be expected. In MoS_2, the bond energy of Mo-S bond is 2.56 eV. From Fig. 2, the bond energy of Cu-S bond is 0.97 eV for Cu-adsorption on 1T'-MoS_2 with the

concentration of 4%. With the formula (3) above, the configuration of transferred charges between Cu-S is difficult to distinguish (Fig. S6 in SI). We define the charge redistribution with the adsorption of Cu by the formula,

$$\Delta\rho'(r) = \rho_{\text{total}}(r) - \rho_{MoS_2}(r) - \rho_{Cu}(r), \quad (4)$$

with the charge density of MoS_2 as the reference state. As shown in Fig. 7b and 7e, the adsorption of Cu with low concentration indicates that there is an electron accumulation between Cu and S. The electron charge transferred in 1T' case is clearly large in comparison with the 2H case. The case of high adsorption concentration (Fig. 7c and 7f) is similar. This charge transfer also explains the stronger interaction between Cu and MoS_2 in 1T' phase, compared to that in 2H phase. This does not rely on destabilization of the 2H structure by occupation of antibonding states, since for weakly electropositive Cu, a strong electron transfer does not occur in the 2H structure. This is in contrast to alkali metals. The electronic structure for Li adsorption on 2H MoS_2 (supplemental, Fig. S7), shows that Li s orbitals contribute to the electronic structure well above the conduction band minimum of 2H MoS2 and that the Fermi level shifts into the Mo d antibonding conduction band states upon Li adsorption.

Thus, we find that the adsorption of Cu can induce the 2H – 1T' structural transformation of MoS_2 via a different mechanism from alkali metals. This is important because Cu is much more chemically inert than alkali metals, which may be important for synthesis, handling, characterization and devices. It may be speculated that other elements near Cu in the periodic table may also induce the transformation. In order to test this, we did calculations of the energetics at 25% coverage for Ag, Au, Ni, Pt and Pd, as given in Table 2. As seen, none of these

elements is as effective as Cu and none induces the transformation at the coverage studied. In these calculations of adsorption with small energy difference, the dispersion force may not be ignored. Here we also consider the contribution of vdW force to the adsorption energy by using optPBE-vdw. As shown in Table 2, the energy difference between 2H and 1T' in Cu case is reduced by vdW force and the difference from 0.081 eV (PBE level) to 0.015 eV (optPBE-vdW). For other metals considered, the energy difference is also reduced with the vdW correction, besides the case of Pt adsorption. From these calculations, It is confirmed further that Cu seems to be special among the considered metals.

4. Conclusions

Cu adsorption on MoS_2 monolayers with different structures is studied using first principles calculations. It is found that the Cu atoms energetically prefer to be adsorbed on the top site of Mo atoms in both the 2H phase and 1T' phases and that Cu adsorption can result in transformation of MoS_2 from 2H to 1T'. This occurs when the adsorption concentration reaches approximately 13%. This is not a strain effect. We explored the path way and energy barrier of phase transition from 2H to 1T'. The main mechanism is the gliding of S atoms on upper surface by passing through the bridge of both nearby Mo atoms. The energy barrier is 1.3 eV per formula cell for pristine MoS_2 and it decreases to 0.9 eV per formula cell under the condition of copper adsorption. The origin of the induced transformation is charge transfer from adatom to the host when the copper is adsorbed on the 1T' surface of MoS_2. This mechanism in which charge transfer in the 1T' adsorbed system favors that structure, even though this charge transfer does

not occur in the 2H phase is distinct from the case of alkali metal adsorption, where there is charge transfer in both structures. It provides an opportunity to tune the structure and therefore electronic and optical properties. Furthermore, because of the distinct charge states of Cu in the two structures it may offer opportunities for obtaining distinct chemical behaviors by structural tuning.

Electronic supplementary information (ESI) available:
Band structures of 2H-MoS_2, 1T'-MoS_2, Cu-adsorbed 2H-MoS_2 and Cu-adsorbed 1T'-MoS_2. Partial density of states and 3D distribution of charge density differences of Cu-adsorbed 2H-MoS_2 and Cu-adsorbed 1T'-MoS_2.

Acknowledgements
The research was supported by the National Key R&D Program of China (Grant No. 2016YFA0200400) and the National Natural Science Foundation of China (Grant No. 11504123 and No.51627805). Work at the University of Missouri was supported by the Department of Energy through the MAGICS Center, Award DE-SC00014607.

References

1 B. Radisavljevic, A. Radenovic, J. Brivio, V. Giacometti and A. Kis, Single-layer MoS_2 transistors, *Nat. Nanotechnol.*, 2011, **6**, 147-150.

2 R. Ganatra and Q. Zhang, Few-Layer MoS_2: A Promising Layered Semiconductor, *ACS nano*, 2014, **8**, 4074–4099.

3 D. Jariwala, V. K. Sangwan, L. J. Lauhon, T. J. Marks and M. C. Hersam, Emerging Device Applications for Semiconducting Two-Dimensional Transition Metal Dichalcogenides, *ACS nano*, 2014, **8**, 1102–1120.

4 H. Fang, S. Chuang, T. C. Chang, K. Takei, T. Takahashi and A. Javey, High-performance single layered WSe_2 p-FETs with chemically doped contacts, *Nano Lett.*, 2012, **12**, 3788-3792.

5 Z. Q. Fan, X. W. Jiang, J. W. Luo, L. Y. Jiao, R. Huang, S. S. Li and L. W. Wang, In-plane Schottky-barrier field-effect transistors based on 1T/2H heterojunctions of transition-metal dichalcogenides, *Phys. Rev. B.*, 2017, **96**, 165402.

6 T. Cao, G. Wang, W. Han, H. Ye, C. Zhu, J. Shi, Q. Niu, P. Tan, E. Wang, B. Liu *et al.*, Valley-selective circular dichroism of monolayer molybdenum disulphide, *Nat. Commun.*, 2012, **3**, 887.

7 G. Eda, H. Yamaguchi, D. Voiry, T. Fujita, M. Chen and M. Chhowalla, Photoluminescence from chemically exfoliated MoS_2, *Nano Lett.*, 2011, **11**, 5111-5116.

8 W. J. Yu, Y. Liu, H. Zhou, A. Yin, Z. Li, Y. Huang and X. Duan, Highly efficient gate-tunable photocurrent generation in vertical heterostructures of layered materials, *Nat. Nanotechnol.*, 2013, **8**, 952-958.

9 H. Li, S. Wang, H. Sawada, G. G. Han, T. Samuels, C. S. Allen, A. I. Kirkland, J. C. Grossman and J. H. Warner, Atomic Structure and Dynamics of Single Platinum Atom Interactions with Monolayer MoS_2, *ACS nano*, 2017, **11**, 3392-3403.

10 Y. C. Lin, D. O. Dumcenco, H. P. Komsa, Y. Niimi, A. V. Krasheninnikov, Y. S. Huang and K. Suenaga, Properties of individual dopant atoms in single-layer MoS_2: atomic structure, migration, and enhanced reactivity, *Adv. Mater.*, 2014, **26**, 2857-2861.

11 T. B. Rawal, D. Le and T. S. Rahman, Effect of Single-Layer MoS_2 on the Geometry, Electronic Structure, and Reactivity of Transition Metal Nanoparticles, *J. Phys. Chem. C.*, 2017, **121**, 7282-7293.

12 J. Shi, D. Ma, G. F. Han, Y. Zhang, Q. Ji, T. Gao, J. Sun, X. Song, C. Li, Y. Zhang *et al.*, Controllable Growth and Transfer of Monolayer MoS_2 on Au Foils and Its Potential Application in Hydrogen Evolution Reaction, *ACS nano*, 2014, **8**, 10196–10204.

13 V. Nicolosi, M. Chhowalla, M. G. Kanatzidis, M. S. Strano and J. N. Coleman, Liquid Exfoliation of Layered Materials, *Science*, 2013, **340**, 1226419.

14 D. YANG and R. F. FRINDT, Li-intercalation and exfoliation of WS_2, *J. Phys. Chem. Solids*, 1996, **57**, 1113-1116.

15 J. A. Wilson and A. D. Yoffe, The transition metal dichalcogenides discussion and interpretation of the observed optical, electrical and structural properties, *Adv. Phys.*, 1969, **18**, 193-335.

16 L. F. Mattheiss, Band Structures of Transition-Metal-Dichalcogenide Layer Compounds, *Phys. Rev. B.*, 1973, **8**, 3719-3740.

17 Q. H. Wang, K. Kalantar-Zadeh, A. Kis, J. N. Coleman and M. S. Strano, Electronics and

optoelectronics of two-dimensional transition metal dichalcogenides, *Nat. Nanotechnol.*, 2012, **7**, 699-712.

18 R. B. Somoano, V. Hadek and A. Rembaum, Alkali metal intercalates of molybdenum disulfide, *J. Chem. Phys.*, 1973, **58**, 697-701.

19 O. Kohulák and R. Martoňák, New high-pressure phases of $MoSe_2$ and $MoTe_2$, *Phys. Rev. B.*, 2017, **95**, 054105.

20 H. P. Komsa and A. V. Krasheninnikov, Two-Dimensional Transition Metal Dichalcogenide Alloys: Stability and Electronic Properties, *J. Phys. Chem. Lett.*, 2012, **3**, 3652-3656.

21 X. Fan, C. H. Chang, W. T. Zheng, J.-L. Kuo and D. J. Singh, The Electronic Properties of Single-Layer and Multilayer MoS_2 under High Pressure, *J. Phys. Chem. C.*, 2015, **119**, 10189-10196.

22 S. Song, D. H. Keum, S. Cho, D. Perello, Y. Kim and Y. H. Lee, Room Temperature Semiconductor-Metal Transition of $MoTe_2$ Thin Films Engineered by Strain, *Nano Lett.*, 2016, **16**, 188-193.

23 N. Luo, C. Si and W. Duan, Structural and electronic phase transitions in ferromagnetic monolayer VS_2 induced by charge doping, *Phys. Rev. B.*, 2017, **95**, 205432.

24 Y. Kang, S. Najmaei, Z. Liu, Y. Bao, Y. Wang, X. Zhu, N. J. Halas, P. Nordlander, P. M. Ajayan, J. Lou *et al.*, Plasmonic hot electron induced structural phase transition in a MoS_2 monolayer, *Adv. Mater.*, 2014, **26**, 6467-6471.

25 G. Gao, Y. Jiao, F. Ma, Y. Jiao, E. Waclawik and A. Du, Charge Mediated Semiconducting-to-Metallic Phase Transition in Molybdenum Disulfide Monolayer and Hydrogen Evolution Reaction in New 1T′ Phase, *J. Phys. Chem. C.*, 2015, **119**, 13124-13128.

26 Y. Wang, J. Xiao, H. Zhu, Y. Li, Y. Alsaid, K. Y. Fong, Y. Zhou, S. Wang, W. Shi, Y. Wang *et al.*, Structural phase transition in monolayer $MoTe_2$ driven by electrostatic doping, *Nature*, 2017, **550**, 487-491.

27 M. Kan, J. Y. Wang, X. W. Li, S. H. Zhang, Y. W. Li, Y. Kawazoe, Q. Sun and P. Jena, Structures and Phase Transition of a MoS_2 Monolayer, *J. Phys. Chem. C.*, 2014, **118**, 1515-1522.

28 S. Jiménez Sandoval, D. Yang, R. F. Frindt and J. C. Irwin, Raman study and lattice dynamics of single molecular layers of MoS_2, *Phys. Rev. B.*, 1991, **44**, 3955-3962.

29 G. Eda, T. Fujita, H. Yamaguchi, D. Voiry, M. Chen and M. Chhowalla, Coherent Atomic and Electronic Heterostructures of Single-Layer MoS_2, *ACS nano*, 2012, **6**, 7311–7317.

30 Y. C. Lin, D. O. Dumcenco, Y. S. Huang and K. Suenaga, Atomic mechanism of the semiconducting-to-metallic phase transition in single-layered MoS_2, *Nat. Nanotechnol.*, 2014, **9**, 391-396.

31 H. H. Huang, X. F. Fan, D. J. Singh, H. Chen, Q. Jiang and W. T. Zheng, Controlling phase transition for single-layer MTe_2 (M = Mo and W): modulation of the potential barrier under strain, *Phys. Chem. Chem. Phys.*, 2016, **18**, 4086-4094.

32 A. V. Kolobov, P. Fons and J. Tominaga, Electronic excitation-induced semiconductor-to-metal transition in monolayer $MoTe_2$, *Phys. Rev. B.*, 2016, **94**, 094114.

33 Y. Zhou and E. J. Reed, Structural Phase Stability Control of Monolayer $MoTe_2$ with Adsorbed Atoms and Molecules, *J. Phys. Chem. C.*, 2015, **119**, 21674-21680.

34 P. Wu, N. Yin, P. Li, W. Cheng and M. Huang, The adsorption and diffusion behavior of noble metal adatoms (Pd, Pt, Cu, Ag and Au) on a MoS_2 monolayer: a first-principles study, *Phys. Chem. Chem. Phys.*, 2017, **19**, 20713-20722.

35 G. Kresse and J. Furthmuller, Efficient iterative schemes for ab initio total-energy calculations using a plane-wave basis set, *Phys. Rev. B.*, 1996, **54**, 11169-11186.

36 J. P. Perdew, K. Burke and M. Ernzerhof, Generalized Gradient Approximation Made Simple, *Phys. Rev. Lett.*, 1996, **77**, 3865-3868.

37 H. J. Monkhorst and J. D. Pack, Special points for Brillouin-zone integrations, *Phys. Rev. B.*, 1976, **13**, 5188-5192.

38 M. Dion, H. Rydberg, E. Schröder, D. C. Langreth and B. I. Lundqvist, Van der Waals density functional for general geometries, *Phys. Rev. Lett.*, 2004, **92**, 246401.

39 J. Klimeš, D. R. Bowler and A. Michaelides, Chemical accuracy for the van der Waals density functional, *J. Phys.: Cond. Matt.*, 2010, **22**, 022201.

40 A. V. Krukau, O. A. Vydrov, A. F. Izmaylov and G. E. Scuseria, Influence of the exchange screening parameter on the performance of screened hybrid functionals, *J. Chem. Phys.*, 2006, **125**, 224106.

41 D. M. Guzman, N. Onofrio and A. Strachan, First principles investigation of copper and silver intercalated molybdenum disulfide, *J. Appl. Phys.*, 2017, **121**, 055703.

42 W. G. Dawson and D. W. Bullett, Electronic structure and crystallography of $MoTe_2$ and WTe_2, *J. Phys. C: Solid State Phys.*, 1987, **87**, 6159-6174.

Table 1

Table 1. Adsorption concentration of Cu and charges per formula unit transferred from Cu to MoS_2 surface for 2H phase and 1T' phase from Bader charge analysis, respectively. The concentrations are in terms of atomic percent relative to the total number of atoms.

concentration	Charges (e/f.u.)	
	2H	1T'
4%	0.05	0.07
5.3%	0.06	0.09
7.7%	0.10	0.13
10%	0.09	0.16
14.3%	0.17	0.22
20%	0.17	0.26
25%	0.20	0.31

Table 2

Table 2. Energy difference (2H-1T') per formula unit between 2H- MoS_2 and 1T'-MoS_2 with the adsorption of different metals calculated with/without the consideration of vdW effect. (the adsorption concentration is 25%).

Materials	ΔE (eV/f.u)		Materials	ΔE (eV/f.u)	
	PBE	optPBE-vdw		PBE	optPBE-vdw
MoS_2/Ni	-0.186	-0.147	MoS_2/Cu	0.081	0.015
MoS_2/Pd	-0.361	-0.201	MoS_2/Ag	-0.529	-0.480
MoS_2/Pt	-0.030	-0.089	MoS_2/Au	-0.640	-0.600

Figure 1

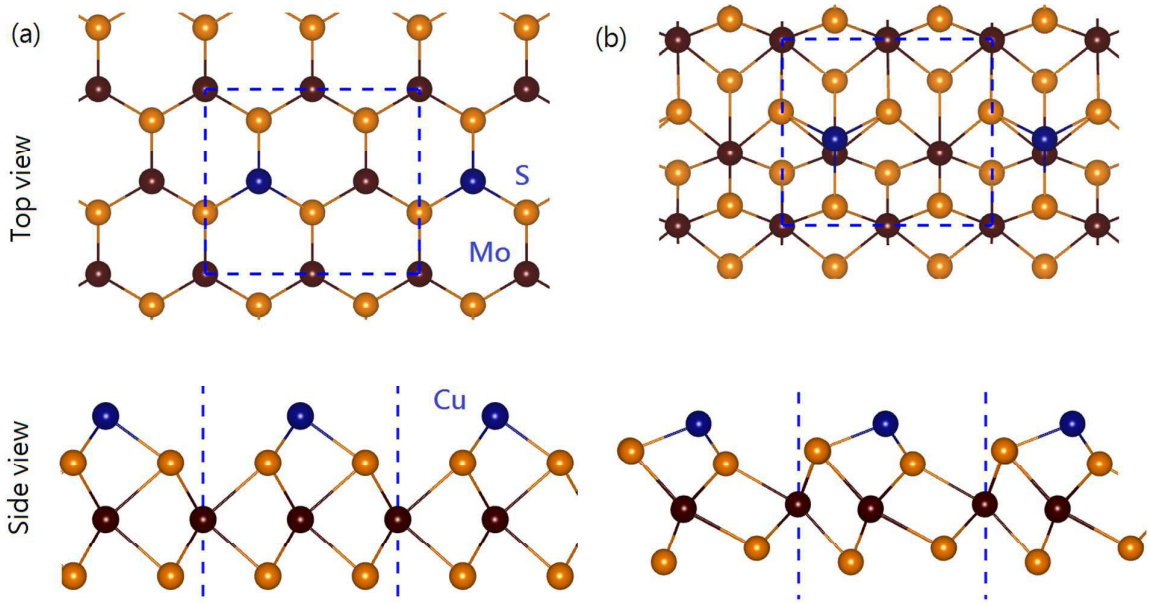

Fig. 1. Top view and side view of the structures of MoS_2 monolayer with the adsorption of a Cu atom in 2x1 rectangular supercell for (a)2H phase and (b) 1T' phase.

Figure 2.

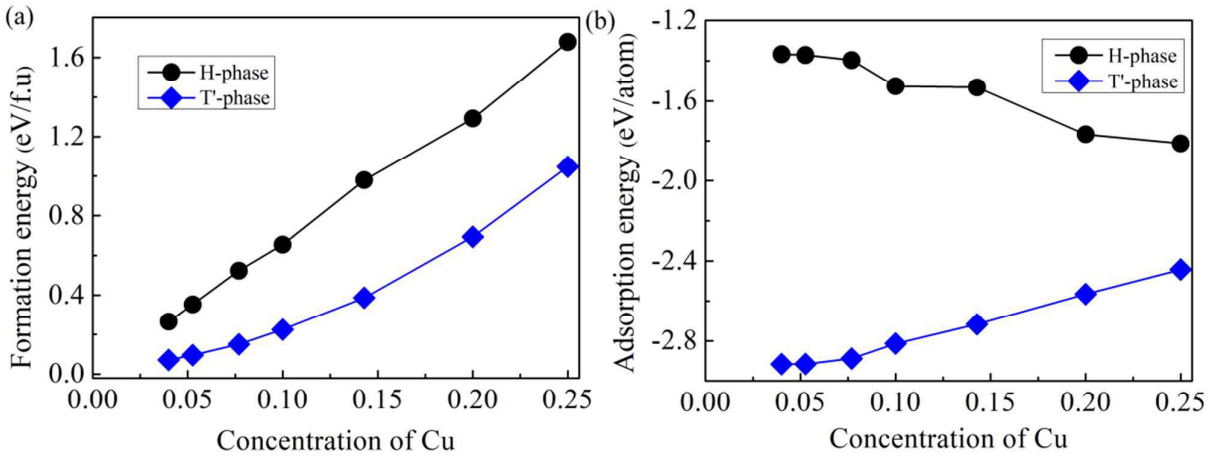

Fig. 2. (a)Formation energy and (b) adsorption energy of MoS_2 monolayer with the adsorption of Cu as a function of the concentration of Cu for 2H and 1T' phases.

Figure 3.

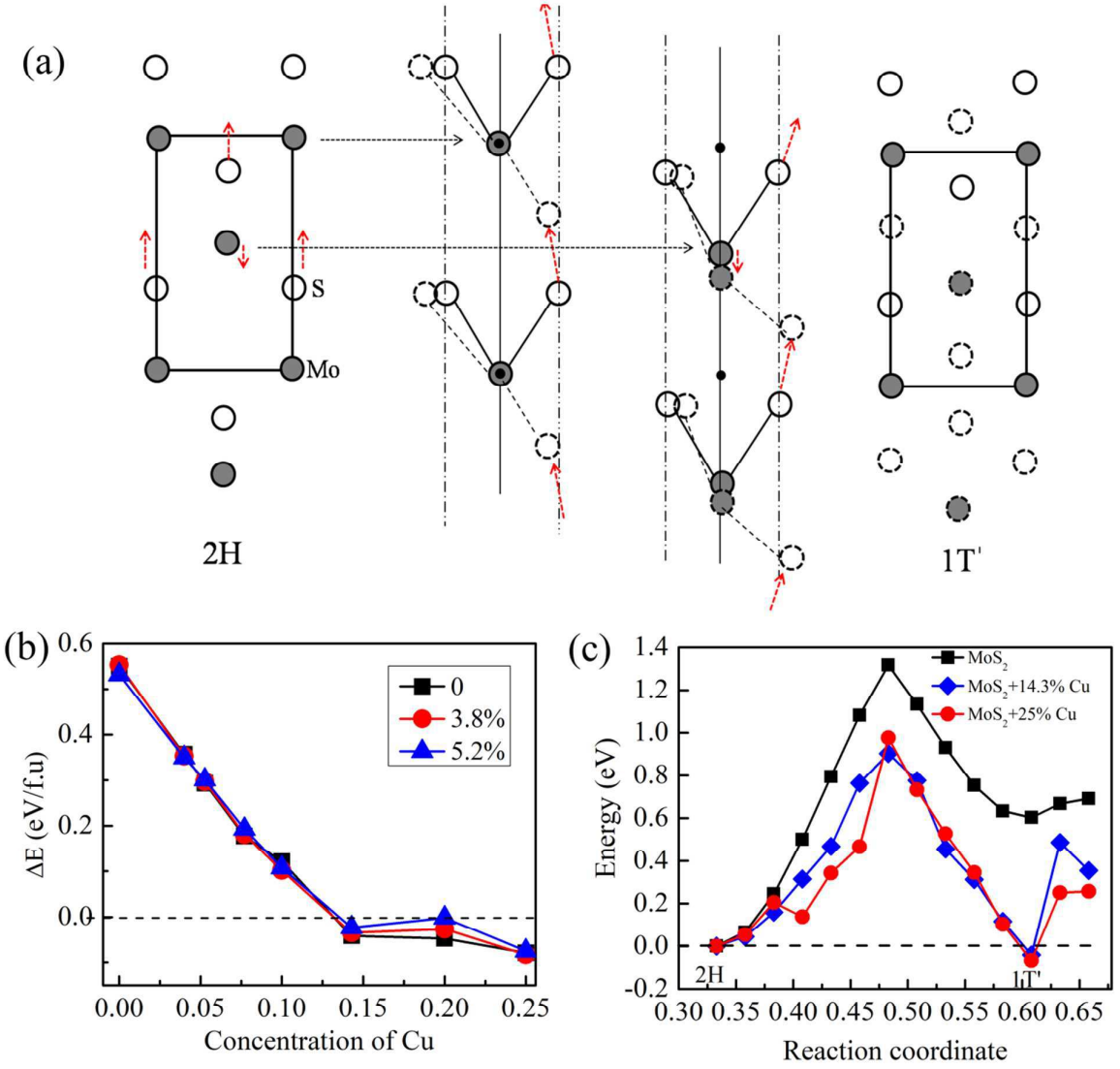

Fig3. (a) Schematic representation of the phase transition from 2H to 1T' phase, (b) the energy difference between 1T' and 2H phase as a function of the adsorbed Cu concentration under the different strains (3.8 % and 5.2 %), compared with zero strain, and the phase transition curve from 2H to 1T' with/without the adsorption of Cu. Note that in (a) the red arrows indicate the direction of moving of atoms (Mo and S), and the full line circles and dotted line circles represent the positions of atoms in the initial state (2H) and that of the final state (1T'), respectively. In (c), the reaction coordinate shows the motion of S atoms on upper surface going through the bridge of nearby two Mo atoms accompanied by local motion of other atoms (two S atoms on lower surface and one Mo atoms in the center of rectangular cell).

Figure 4.

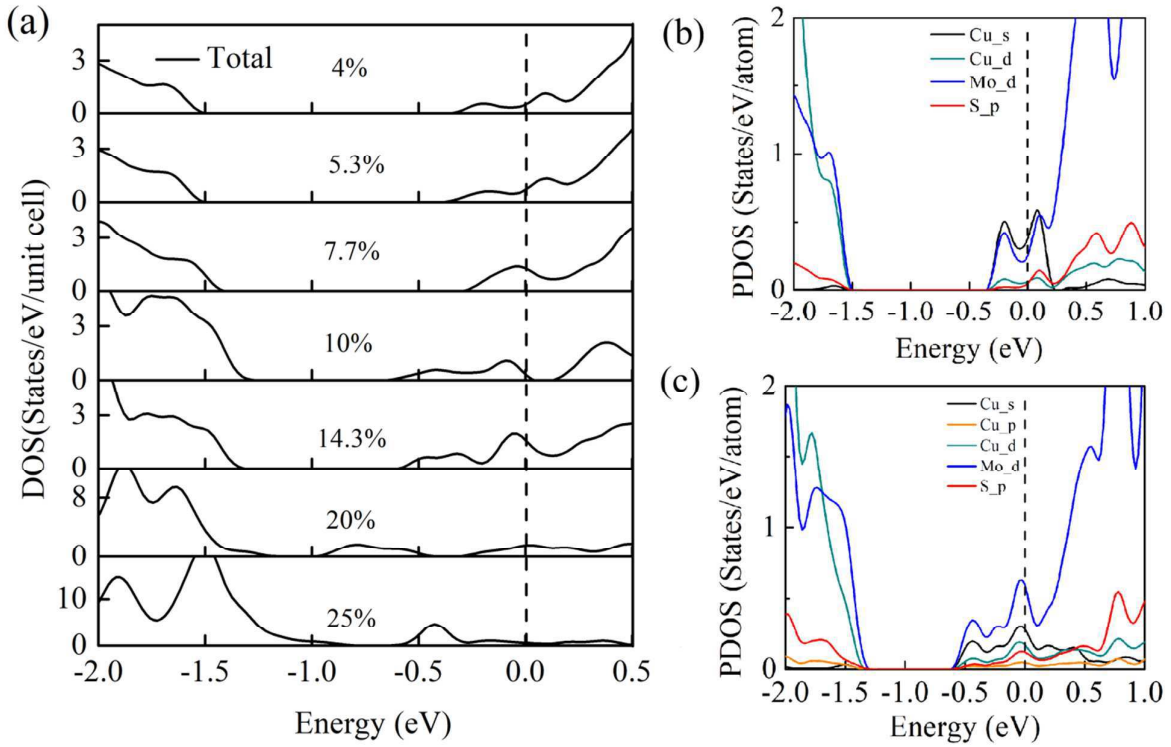

Fig. 4. (a)Density of states(DOS) of 2H-MoS_2monolayer with different contents of Cu adsorbed on the surface, and partial density of states(PDOS) of Cu-adsorbed 2H-$MoS_2$with the concentrations of (b) 4%, and (c) 14.3% at PBE level. The dashed vertical line at 0 eV indicate Fermi level. Note that Cu-adsorption results in the up-shift of Fermi level from top of valance bands into conduction bands.

Figure 5.

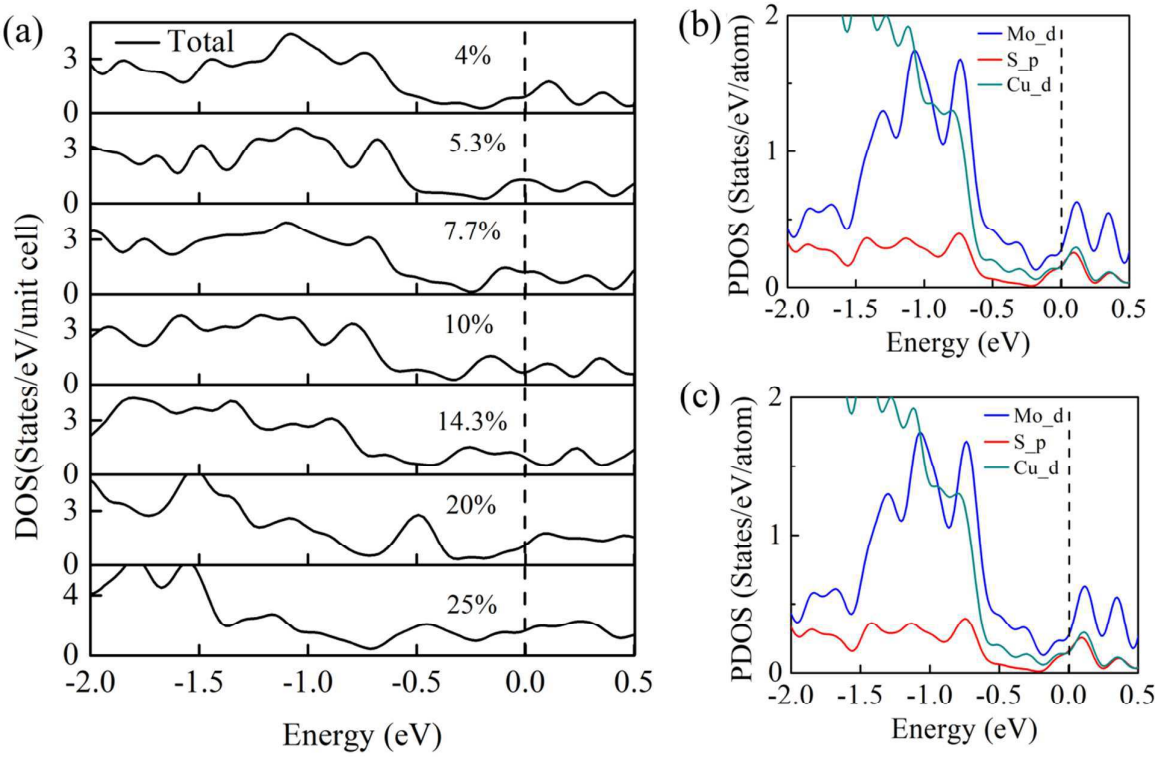

Fig. 5. (a)Density of states(DOS) of 1T'-MoS_2 monolayer with different contents of Cu adsorbed on the surface, and partial density of states(PDOS) of Cu-adsorbed 1T'-$MoS_2$with the concentrations of (b) 4%, and (c) 14.3% at PBE level. The dashed vertical lines indicate Fermi levels.

Figure 6.

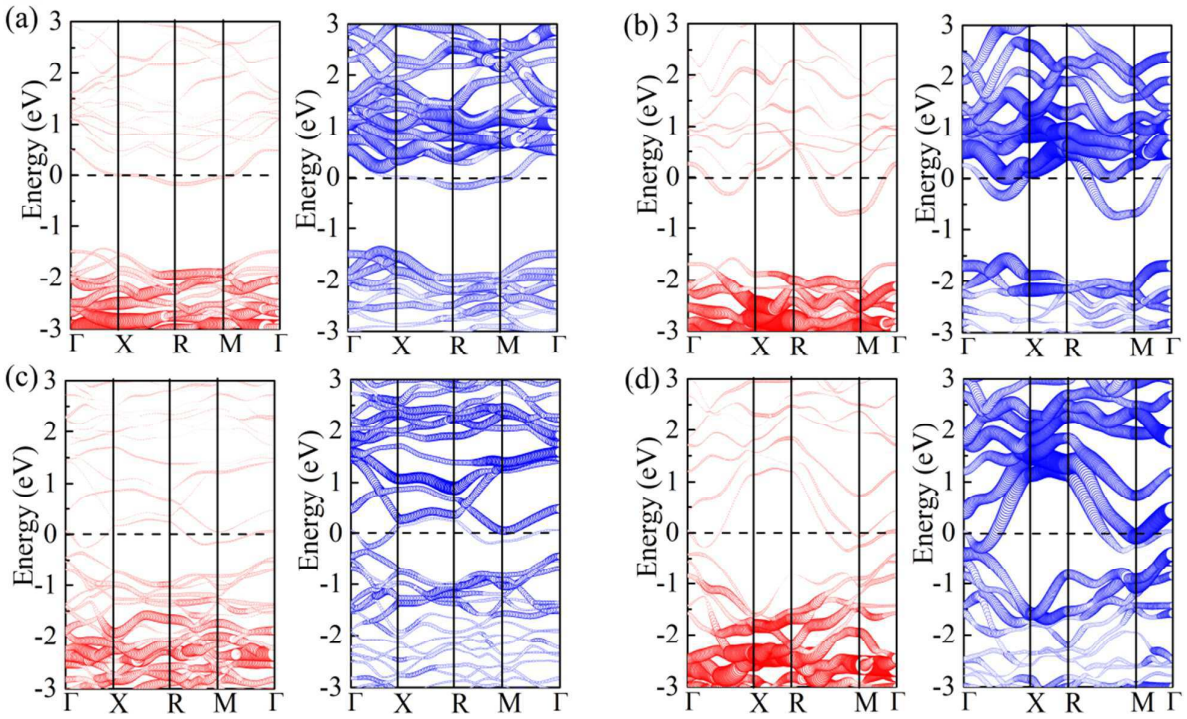

Fig. 6. Electronic band structures of Cu-adsorbed 2H-$MoS_2$with the concentration of (a) 7.7%and (b)14.3% and those of Cu-adsorbed 1T'-MoS_2 with the concentration of (c)7.7% and (d) 14.3% at PBE level. The red bands and blue bands represent the contribution of Cu atoms and Mo atoms, respectively. The symbols Γ, X, R, and M indicate the k-points (0,0,0), (0.5,0,0), (0.5,0.5,0), and (0,0.5,0), respectively. The horizontal dashed line at 0eVdenotes Fermi level.

Figure 7.

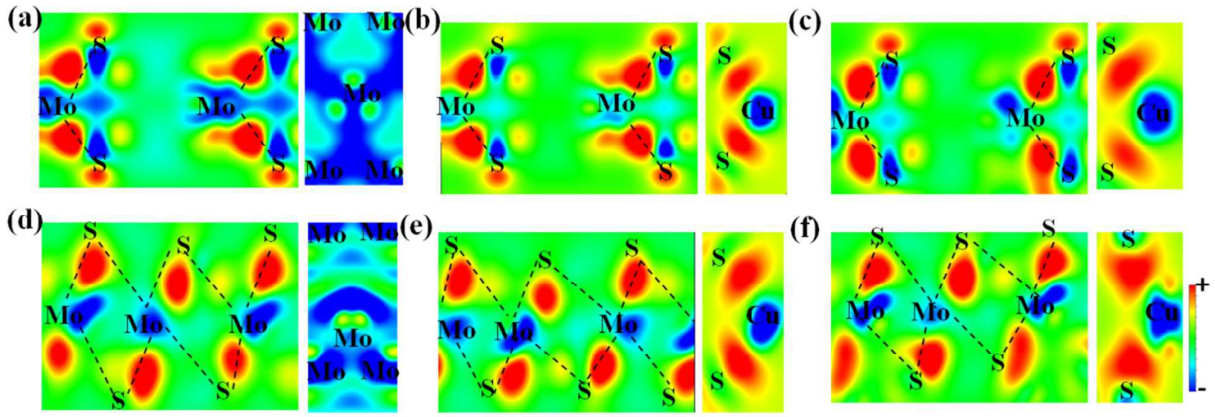

Fig. 7. Distribution of charge density differences of (a) pristine 2H-MoS_2,Cu-adsorbed 2H-MoS_2 with the concentration of (b) 4% and (c) 14.3%, (d) pristine 1T'-MoS_2, and Cu-adsorbed 1T'-MoS_2 with the concentration of (e) 4% and (f) 14.3%, in the vertical plane where the atoms S and Mo pass through, calculated by the formula (3). In (b), (c) (e) and (f), the charges between Cu and S are presented by the charge redistribution with the formula (4). The red color and blue color represent the charge accumulation, and charge depletion, respectively.